To appear in the *Journal of Geophysical Research*, 2000.

A critical height of quiescent prominences before eruption

Boris P. Filippov, and O Gym Den
Institute of Terrestrial Magnetism, Ionosphere and Radio Wave Propagation, Russian Academy of Sciences, Troitsk, Moscow Region, Russia

Abstract

We discuss the problem of the limiting height of quiescent prominences and the relationship of this value to the photospheric magnetic field characteristics. Solar prominences are considered as pre-eruptive states of CMEs. We note that in a model of inverse polarity filament, the equilibrium is stable only in the region where the photospheric magnetic field falls off with a height not faster than h^{-1}. Current-free magnetic field calculations are compared with the observed prominence heights. It is shown that the maximum stable height of a prominence depends on the vertical gradient value and never exceeds the level where the power is equal to unity in the power-low decrease of the magnetic field. This is a new way to predict prominence eruptions and CMEs.

1. Introduction

We do not know for certain what is the pre-eruptive stage of a coronal mass ejection. Many CMEs originate from a disruption of the coronal helmet streamers [*Illing and Hundhausen,* 1986; *Hundhausen,* 1993] while there are clear examples of CMEs that are not caused by the disruption of helmet streamers [*Andrews et al.,* 1999]. In many cases CMEs contain rather compact bright cores, which are believed to be the remnants of eruptive prominences [*Crifo et al.,* 1983; *Sime et al.,* 1984; *Hundhausen,* 1999]. The bright core is surrounded by a dark cavity of depleted material and the cavity is bordered with a bright loop of enhanced density. The CME loop may actually be the skyplane projection of a 3-D, shell-like structure. The top of the prominence observed in either the Hα emission or the scattered white light almost always moves outward more slowly than the top of the dark cavity or the bright frontal loop. This fact has been used against the concept that the prominence eruption drives the coronal mass ejection [*Hundhausen,* 1999]. However, assuming that a prominence and a cavity are two different parts of the same magnetic flux rope [*Low,* 1996], the difference in velocity of the central part of the rope (prominence) and its outer part (cavity) is reasonable [*Filippov,* 1996]. To reinforce this concept, it is necessary to know the form and the strength of the magnetic field in the cavity. Unfortunately, direct observational information on the cavity is scarce since its emissions are weak. In contrast, the prominence material reveals the flux rope not only on the limb but also on the disk as a twisted filament.

Statistical association studies typically indicate that CMEs are most frequently associated with a near-surface activity in the form of erupting filaments [*Munro et al.,* 1979; *Webb and Hundhausen*, 1987; *St. Cyr and Webb*, 1991]. There is no doubt that an ascending filament current, as a source of magnetic field, should make an appreciable rearrangement of coronal density in the large volume surrounding an eruptive filament. In the region where magnetic pressure is greater than gas pressure ($\beta < 1$), plasma motion can be assumed as a drift or a frozen-in motion. Its characteristic is such that the further one gets from the filament, the larger is the drift velocity of the plasma. This type of motion leads to a rarefaction of the plasma and a growing of a cavity around the filament. Near the boundary $\beta = 1$, gas pressure begins to slowdown plasma motion and, as a result, the coronal density increases. Plasma compression near the surface $\beta = 1$ leads to the formation of a dense envelope, which can be identified with the outer loop of a CME [*Filippov,* 1996].

Solar prominences can be considered [*Engvold*, 2000] as pre-eruptive states of CMEs. For some CMEs, the onset of the ejection affects the filament equilibrium. How can we estimate the stability of any observed filament and the probability of its eruption? What parameters do we need for this purpose?

2. Filament Equilibrium and Stability

We know that the height of a filament increases with its age [*Rompolt,* 1990]. The death of a filament is usually an eruption. According to *Zirin* [1979], prominences that exceed more or less 50 Mm in height are inclined to erupt. An eruption usually takes place within two days after the prominence reaches the threshold height. The filament height, then, can be a measure of its age and its readiness for eruption. For the quantitative description, however, we need a scale to estimate whether a filament is sufficiently high or low. We believe that we can compare the filament height with the vertical scale length of the magnetic field of sub-photospheric sources in the corona.

From the magnetostatic standpoint, there are two types of filament equilibrium represented by normal polarity models and inverse polarity models. They differ mainly in the electric current direction relative to the external magnetic field. In the first type, represented by the *Kippenhahn-Schluter* [1957] model, the Lorenz force is directed upward and balances the weight of a filament. In the second type, represented by the *Kuperus-Raadu* [1974] model one part of the Lorenz force is directed downward, and the only supporting force is a repulsion of the current from the currents induced on the surface of the photosphere. Inverse polarity models have a number of advantages in solving the problems of a filament stability, an internal fine structure, a storage of magnetic energy, and the filament acceleration during eruption. Measurements of the magnetic field in prominences reveal the inverse polarity in the majority of them [*Demoulin,* 1998].

The mentioned above two classes of models include a wide variety of modifications and improvements. The obvious generalization is to take into account the third component of the magnetic field directed along the filament axis, the more so as the magnetic field measurements and filament structure reveal the axial component to be the strongest [*Leroy,* 1989; *Martin,* 1998]. This way, the inverse polarity model transforms into a flux rope model [*Priest et al.,* 1989; *Low and Hundhausen,* 1995; *Aulanier and Demoulin,* 1998]. Since plasma parameter β is less than 1, coronal magnetic configurations are not far from force-free state. A field-aligned current in the polarity inversion zone should be directed along the inversion line. After the loss of equilibrium, the configuration is no more force-free. For our purpose we do not need a detailed internal distribution of the magnetic field or the electric current inside a flux rope. All we need is the equilibrium of a filament as a whole, which depends mainly on the total axial current. We can restrict our consideration, therefore, to a simple, two-dimensional model with the line current that represents the integral axial current of the flux rope.

We had studied the problem of prominence height distribution [*Filippov and Den*, 2000; *Den and Filippov* , 2000] and found that a finite size filament, with the current directed in accordance with Kippenhahn–Schluter model, is unstable even in the magnetic field with the upward-concave shape of field lines. An opposite direction current is stable against horizontal perturbations in a downward-concave magnetic structure [*Van Tend and Kuperus*, 1978]. The stability against vertical perturbations of the current position depends on the distribution of the photospheric magnetic field $B(h)$ above the polarity inversion line. In a simple, two-dimensional inverse-polarity model, the force per unit length of the filament, acting in the vertical direction, is [*Van Tend and Kuperus*, 1978]

$$F = \frac{I^2}{c^2\,h} - \frac{I}{c}\,B(h) - mg, \tag{1}$$

where B is the potential field corresponding to the photospheric flux distribution, and I is the the filament electric current located at height h above the neutral line. The second term on the right-hand side represents the part of the total Lorentz force that is due to the potential "background field," and the first term represents the remaining part that is due to currents induced in the photosphere (which can be described by a subphotospheric mirror current). These two parts of the Lorentz force are directed downward and upward, respectively. The filament weight mg is sufficient only for equilibrium of very low filaments with weak currents. For high filaments which are ready for eruption, the gravitational term may be ignored. Really, it is follows from Equation (1) that in equilibrium

$$I > B\,c\,h. \tag{2}$$

Therefore, a lower limit on the upward Lorentz force associated with the photospheric currents is

$$F_B = \frac{I}{c}\,B > B^2\,h. \tag{3}$$

For the typical values of $B = 5$ G and $h = 3 \cdot 10^9$ cm (see, for example, Table 1), it gives $F_B > 7.5 \cdot 10^{10}$ dyne. The mass $m = 2.5 \cdot 10^6$ g per unit length of the filament, needed to counterbalance such a force, is an order of magnitude larger than what is typically inferred from observations (reference). We, therefore, conclude that the gravity term may be left out in Equation (1), so that the total force balance involves only the two Lorentz force terms.

If the filament weight is disregarded, the equilibrium is achieved at height h_0 determined from the equation

$$\frac{I}{c\,h_0} = B(h_0). \tag{4}$$

The equilibrium is known to be stable if the second derivative of potential energy is positive,

$$\left.\frac{d^2W}{dh^2}\right|_{h_0} = -\left.\frac{dF}{dh}\right|_{h_0} > 0. \tag{5}$$

Substituting (1) and (4) in (5), we obtain

$$\left.\frac{dB}{dh}\right|_{h_0} > -\frac{B(h_0)}{h_0}. \tag{6}$$

Hence, the filament equilibrium is stable if the vertical gradient in external field lies in the range

$$-\frac{B(h_0)}{h_0} < \left.\frac{dB}{dh}\right|_{h_0} < 0. \tag{7}$$

If the change of the magnetic field in some range of heights is described by a power-law function

$$B(h) = Ch^{-\alpha}, \tag{8}$$

where

$$\alpha = -\frac{h}{B}\frac{dB}{dh}, \tag{9}$$

then we find from (6) that

$$\alpha < 1. \tag{10}$$

That the vertical gradient for the vertical stability should be negative is consistent with the downward-concave shape of field lines needed for the horizontal stability in the potential magnetic field with the sources located beneath the photosphere. The condition obtained for the vertical stability is very clear, bearing in mind that the magnetic field of the "mirror" current varies in inverse proportion to h. Real solar magnetic fields may have a very complicated height dependence, determined by the distribution of the field sources in the photosphere. This dependence reflects the scale of the sources that dominate at a given level. If, beginning from a height h_c, the field falls off faster than $\sim h^{-1}$, then it is the critical height for quiescent filaments. This critical point of stability was at first found by *Van Tend and Kuperus* [1978]. In models in which the external field is simulated by a linear bipole, the critical height corresponds to the depth at which the bipole lies beneath the photosphere [*Molodensky and Filippov*, 1987; *Martens and Kuin*, 1989].

3. Magnetic Field Calculations

We determined the filament positions and the prominence heights from Hα filtergrams of the Big Bear Solar Observatory and Ca II K_3 spectroheliograms of the Meudon Observatory (available at http://sohodb.nascom.nasa.gov/synoptic/gif/). The upper edge of a prominence is assumed as the prominence height in this case. It may coincide with the top of the filament arch, or be the height of the intermediate part of the filament, depending on the projection of the filament body on the limb. An uncertainty ± 5 Mm, indicated in Table 1, corresponds to the measurement accuracy of the upper edge of the visible in a filtergram prominence . Of course, the uncertainty in determining the actual height of the filament arch is even higher. By using a very simple, two-dimensional model for the filament equilibrium, we hope that with sufficient statistics we can improve the reliability of the comparison of the calculated and measured values.

It is very difficult to measure coronal magnetic field. Measurements can be made using either the Zeeman effect or the Hanle polarization effect in the hydrogen and helium emission lines that originate in the dense material (prominences). Sometimes, it is possible to measure the magnetic field in the low corona above sunspots using infrared lines or radio gyro lines. The coronal magnetic field is usually calculated by extrapolating the field from the photospheric level. The potential magnetic field in the corona can be found by solving the Neumann external boundary-value problem. There are a number of methods to solve numerically this problem [*Altschuler and Newkirk*, 1969; *Levine*, 1975; *Adams and Pneuman*, 1976]. The first code was developed and successfully used by *Schmidt*, [1964]. Since we are concerned with the magnetic field at the prominence height, which is small compared to the solar radius, we may neglect sphericity and use the well-known solution for half-space with a plane boundary (see, e.g., [*Tikhonov and Samarskii*, 1972])

$$\mathbf{B} = \frac{1}{2\pi} \int\!\!\int_S \frac{B_n(x', y', 0)\, \mathbf{r}}{r^3}\, dx' dy', \qquad (11)$$

where $B_n(x', y', 0)$ is the normal magnetic-field component on plane S, and $\mathbf{r}$ is the radius vector from a point on the surface to a given point in the corona. The integration can be performed analytically within a small rectangular area with the constant value of $B_n(x', y', 0)$ ([*Den et al.*, 1979]) . This area represents a unit of the spatial resolution of a magnetograph.

We are aiming to find the functional dependence of magnetic field strength B on height h. For this purpose, we need magnetic-field data with a sufficiently high spatial resolution (no worse than $5''$). We used MDI magnetograms of SOHO, which are accessible via Internet at http://sohodb.nascom.nasa.gov/summary/. We cut out a rectangular region around the filament under study from the magnetogram of the full disk and ignore the contribution of the magnetic sources in the areas outside it. This is justified if the region size is much larger than the filament height, or if the main sources of the field (active regions) lie within the cut-out region. In practice, the region sizes were of the order of $10' \times 10'$. As usual, the line-of-sight component of the magnetic field was taken as the normal one, which gives an error mainly at the edges of the region.

We find that it is impossible to measure the filament height and the magnetic field at the same moment. We can only measure the filament height on the limb when a filament is observed as a prominence (Figure 1), whereas the magnetic field below the filament can only be measured on the disk; the best location of the region being near the central meridian. The time gap reaches several days. We can, therefore, only analyze quiescent filaments assuming that the field not changing drastically during this time. Figure 1

4. Results

Consider, for example, the filament that crossed the central meridian on January 11, 2000 (Figure 1). Figure 2 shows the magnetogram of the central part of the northern solar hemisphere on January 11, 2000, obtained with the MDI instrument on SOHO and magnetic field lines calculated on the basis of this magnetogram. The silhouette of the filament is seen on the magnetogram in Figure 2 as a white contour. This is a rather typical quiescent filament located between two active regions NOAA 8821 and NOAA 8826. The structure of the magnetic field near the filament location is a simple arcade stretched along the polarity inversion line. The calculated field is the field generated only by photospheric sources (i.e., a potential field). Although the field of the filament current is not weak compared to the field of the subphotospheric currents, it can be readily separated from the latter. In the inverse-polarity model, the effect of the induction currents on the photospheric surface reduces to neutralizing the normal field component of the filament current on this surface, implying that the field of the coronal currents does not penetrate beneath the photosphere. For this reason, the measured normal field component in the photosphere is entirely determined by the field of the photospheric sources and can be used to calculate its potential extension into the corona.

Figure 2

The structure in the Figure 2 does not represent a strong axial component of the magnetic field observed in the filament channels [*Gaizauskas*, 1998]. We believe that this part of the total magnetic topology is created by interference of the protospheric and coronal magnetic fields in the upper chromosphere. The component of the photospheric field, which is transverse to the polarity inversion line and filament axis, is reduced by the azimuthal field of the filament current. At the center of a flux rope, there is only the axial component of the magnetic field [*Filippov*, 1994]. It is generated both by the photospheric sources and by the azimuthal current of the flux rope. However, this axial magnetic field does not significantly influence the equilibrium of a filament and we do not take it into account in our modeling.

The polarity inversion line is inclined at an angle of about 45° counterclockwise to the meridian. The shape of the line at different heights is presented in Figure 3; it becomes nearly straight above the height of 35 Mm. Figure 4 shows the distribution of the parameter α along the inversion line at different heights. The curve drawn along the humps is shown in Figure 5. The level $\alpha = 1$ defines the limiting height for the filament. Thus, we choose as the critical height the minimal height along the polarity inversion line above which the field falls off faster than h^{-1}.

Figure 3

Figure 4

Figure 5

In Table 1, there is a list of filaments included in the analysis. The first column shows the date of a filament crossing the central meridian. Next come the prominence height, the critical height, and the calculated magnetic field. The results are more illustrative in the plot, where one axis is the prominence height and the other is the critical height (Figure 6). Bisector, therefore, shows the limit of stability. The filaments that safely passed the west limb are marked with the solid circles, while the filaments that disappeared from the disk (see examples in Figure 7), are marked with the open circles. It seems that the solid circles more or less evenly fill the angle between the bisector and the horizontal axis, while the open circles tend to cluster about the bisector. This shows that eruptive prominences were near the limit of stability a few days before an eruption.

Table 1

Figure 6

Figure 7

5. Discussion and Conclusions

If CMEs are driven magnetically, the most likely field configuration of a CME is a flux rope embedded in an arcade of field lines of the photospheric sources. An electric current in the flux rope accumulates energy in excess of the potential magnetic field energy, which could easily be transformed into the kinetic energy of accelerated CME material. Most of the flux rope volume coincides with a coronal cavity, an object difficult for observations due to the notably reduced emission. On the other hand, cool prominence material, which is believed to be contained in the bottom part of the flux rope, is easily observable with the ground-based telescopes. Thus, solar prominences can be treated as the tracers of flux ropes and electric currents in the corona. Figure 8 shows a typical relationship between a prominence and a cavity. Two prominences visible in absorption in the EUV image are located in the lower part of the ring-like cavities surrounded by near-circular coronal bright loops. The pattern is most clear for the high-latitude prominence. The prominence material spreads up to the center of the cavity. Thus, the top of the prominence can be considered as the height of the flux rope.

Of course, the presence of the significant amount of prominence material in the flux rope is not the necessary condition for its existence in the corona, but when observed, prominences or filaments can supply us with important information on flux rope characteristics. First of all, it is interesting to know what is the relative value of the total electric current. Is it enough to expect an eruption of the configuration in the nearest future?

In inverse polarity models, the equilibrium height of a filament is related to the value of the filament electric current. The stronger the electric current, the higher the filament. Since the majority of filaments reveal the inverse polarity, we can use the filament height in the estimation of the coronal current. However, the equilibrium and stability of a filament depend not only on its current but also on the characteristics of the external magnetic field. We should, therefore, compare the observed prominence height with a value characterizing the photospheric magnetic field. This value is the critical height, which can be found in the distribution of the magnetic field vertical gradient above the polarity inversion line. In spite of the uncertainties in determination of the filament heights, the simpicity of the model, and restrictions related with the field extrapolation, the two families of filaments – stable quiescent and eruptive – are clearly separated in the Figure 6. We believe that a comparison of the real heights of prominences with the critical heights could be a basis for predicting filament eruptions and following CMEs.

Acknowledgments.

B.F. is grateful to the Organizing Commettee of the International Conference on Solar Eruptive Events for the financial support. We wish to thank the unknown referees for critical comments and valuable suggestions and Asst. Managing Editor Dr. E. Arscott for correction of the language of the paper. This work was supported in part by the Russian Foundation for Basic Research (grant 00-02-17736) and Russian State Astronomical Program.

The Editor would like to thank the reviewer of this manuscript.

References

Adams, J., and G.W. Pneuman, A new technique for the determination of coronal magnetic fields. A fixed mesh solution to Laplace's equation using line-of-sight boundary conditions, *Sol. Phys., 46*, 185-203, 1976.

Altschuler, M.D., and G. Newkirk, Magnetic fields and structure of the solar corona. I: Methods of Calculating Coronal Fields, *Sol. Phys., 9*, 131-149,1969

Andrews, M.D., A.-H. Wang, and S.T. Wu, Observations and modeling of an explosive coronal mass ejection as observed by LASCO, *Sol. Phys., 187*, 427-448, 1999.

Aulanier, G., and P. Demoulin, 3-D magnetic configurations supporting prominences, I. The natural presence of lateral feet *Astron. Astrophys., 329*, 1125-1137, 1998

Crifo, F., J.P. Picat, and M. Cailloux, Coronal transients - Loop or bubble, *Sol. Phys., 83*, 143-152, 1983.

Demoulin, P., Magnetic fields in filaments, in *New Perspectives on Solar Prominences, IAU Colloquium 167, ASP Conference Series, Vol. 150*, edited by D. Webb, D. Rust, and B.Schmieder, pp. 78-85, Astron. Soc. of the Pacific, Calif., 1998.

Demoulin, P., and E.R. Priest, A model for an inverse-polarity prominence supported in a dip of a quadrupolar region, *Sol. Phys., 144*, 283-305, 1993.

Den, O.G., O.E. Den, E.A. Kornitskaya, and M.M. Molodenskii, On magnetic field in quiescent prominences, *Solnechnye Dannye*, No. 1, 97-102, 1979

Den, O.G., and B.P. Filippov, On a height of quiescent prominences in the corona, (in press).

Engvold, O., Solar prominences as a pre-eruptive state of CMEs, *J. Geophys. Res., this volume*, 2000.

Filippov, B.P., Fine structure of the chromosphere, *Astron. Lett., 20*, 665-670, 1994.

Filippov, B.P. Coronal mass ejections caused by filament eruptions, *Astron. Astrophys., 313*, 277-284, 1996.

Filippov, B.P., and O.G. Den, Prominence height and vertical gradient in magnetic field, *Astron. Lett., 26*, 322-327, 2000.

Gaizauskas, V., Filament channels: essential ingredients for filament formation, in *New Perspectives on Solar Prominences, IAU Colloquium 167*, ASP Conference Series, vol. 150, edited by D. Webb, D. Rust, and B.Schmieder, pp. 257-264, Astron. Soc. of the Pacific, Calif., 1998

Hundhausen, A.J., Coronal mass ejections, in *The Many Faces of the Sun : a Summary of the Results From NASA's Solar Maximum Mission,* edited by K.T. Strong, J.L.R. Saba, B.M. Haisch, and J. T. Schmelz, p. 143, Springer, New York, 1999.

Hundhausen, A.J., Sizes and locations of coronal mass ejections - SMM observations from 1980 and 1984-1989, *J. Geophys. Res., 98,* 13177-13200, 1993.

Illing, R.M.E., and A.J. Hundhausen, Disruption of a coronal streamer by an eruptive prominence and coronal mass ejection, *J. Geophys. Res., 91,* 10951-10960, 1986.

Kippenhahn, R., and A. Schluter, Eine Theorie der solaren Filamente, *Z. Astrophys., 43*, 36, 1957.

Kuperus, M., and M.A. Raadu, The support of prominences formed in neutral sheets, *Astron. Astrophys., 31*, 189-193, 1974.

Leroy, J.L., Observation of prominence magnetic fields, in *Dynamics and structure of quiescent solar prominences*, edited by E.R. Priest, pp. 77-113, Dordrecht, Kluwer Academic Publishers, 1989.

Levine, R.H., The representation of magnetic field lines from magnetograph data, *Sol. Phys., 44*, 365-370, 1975

Low, B.C., Solar activity and the corona, *Sol. Phys., 167*, 217-256, 1996.

Low, B.C., and J.R. Hundhausen,Magnetostatic structures of the solar corona. II The magnetic topology of quiescent prominences, *Astrophys. J., 443*, 818-836, 1995.

Malherbe, J.M., and E.R. Priest , Current sheet models for solar prominences. I Magnetohydrostatics of support and evolution through quasi-static models, *Astron. Astrophys., 123*, 80-88, 1983.

Martens, P.C.H., and N.P.M. Kuin, A curcuit model for filament eruptions and two-ribbon flares, *Sol. Phys., 122*, 263-302, 1989.

Martin, S.F. Conditions for formation and maintenance of filaments, *Sol. Phys., 182*, 107-137, 1998.

Molodensky, M.M., and B.P. Filippov, Rapid motion of filaments in active regions, *Astron. Zhurn.,* Engl. Transl., *Soviet Astron., 31,* 564-568, 1987.

Munro, R.H., J.T. Gosling, E. Hildner, R.M. Mc Queen, A.E. Poland, and C.L. Ross, The association of coronal mass ejection transients with other forms of solar activity, *Sol. Phys., 61*, 201-215, 1979.

Rompolt B., Small scale structure and dynamics of prominences, *Hvar Obs. Bull., 14*, 37-102, 1990.

Schmidt, H.U., in *NASA symposium on Physics of Solar Flares*, edited by W. Hess, NASA SP-50, 107, 1964.

Sime, D.G., R.M. MacQueen, and A.J. Hundhausen, Density distribution in looplike coronal transients: A comparison of observations and a theoretical model, *J. Geophys. Res., 89,* 2113-2121, 1984.

St. Cyr, O.C., and D.F. Webb, Activity assiciated with coronal mass ejections at solar minimum: SMM observations from 1984-1986, *Sol. Phys., 136*, 379-394, 1991.

Tikhonov, A. N., and A. A. Samarskii, *Equations of Mathematical Physics*, Nauka, Moscow, p. 363, 1972.

Uchida, Y., Yohkoh observations of coronal structures surrounding dark filaments, in *New Perspectives on Solar Prominences, IAU Colloquium 167, ASP Conference Series, Vol. 150*, edited by D. Webb, D. Rust, and B.Schmieder, pp. 163-170, Astron. Soc. of the Pacific, Calif., 1998.

Van Tend, W., and M. Kuperus, The development of coronal electric current system in active regions and their relation to filaments and flares, *Sol. Phys., 59*, 115-127, 1978.

Webb, D.F., and A.J. Hundhausen, Activity associated with the solar origin of coronal mass ejections, *Sol. Phys., 108*, 383-401, 1987.

Zirin, H., The ecology of prominences, in *Physics of Solar Prominences. Proceedings of the IAU Colloquium 44*, edited by E. Jensen, P. Maltby, and F.Q. Orrall, 193-207, 1979.

O.G. Den and B.P. Filippov, IZMIRAN, Troitsk, Moscow Region, 142190, Russia (e-mail: bfilip@izmiran.troitsk.ru)

Received January 0, 0000; revised February 00, 0000; accepted March 00, 0000.

This preprint was prepared with AGU's LATEX macros v5.01. File FilippovPr formatted October 11, 2000.

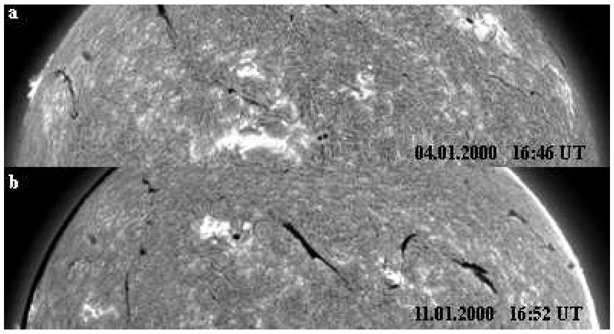

Figure 1. Hα filtergrams showing a filament visible as a prominence above the limb on January 4, 2000 (a) and the same filament on the central meridian on January 11, 2000 (b) (Courtesy of Big Bear Solar Observatory).

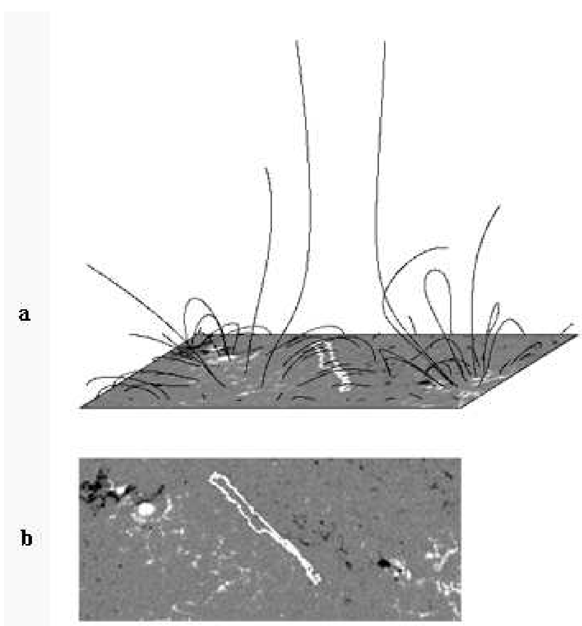

Figure 2. Calculated 3D topology of the coronal magnetic field (a) and the MDI/SOHO magnetogram of the central part of the northern solar hemisphere on January 11, 2000 (b) (Courtesy of the SOHO/MDI Consortium; SOHO is a joint ESA–NASA program).

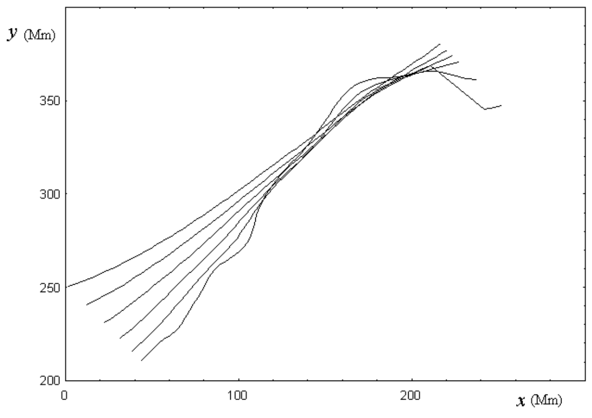

Figure 3. The shape of the polarity inversion line at different heights. The height is increasing with the step 11.6 Mm beginning from the height 17.4 Mm for the curves arranged from bottom to top of the plot.

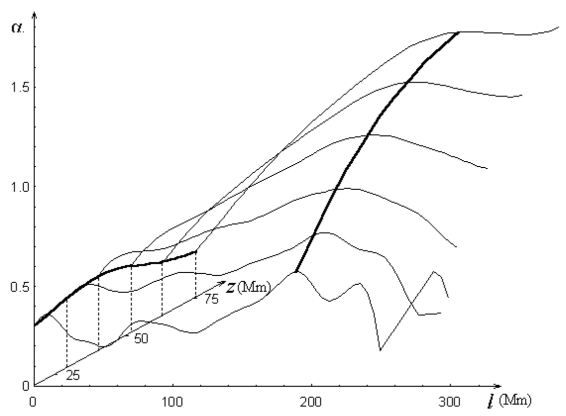

Figure 4. The distribution of the parameter α along the inversion line at different heights.

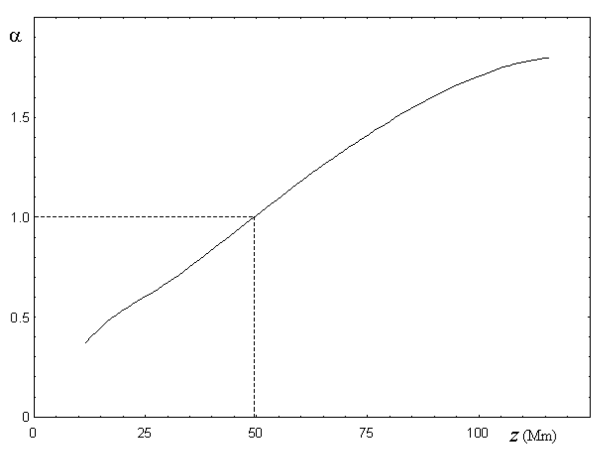

Figure 5. The local index α as a function of height.

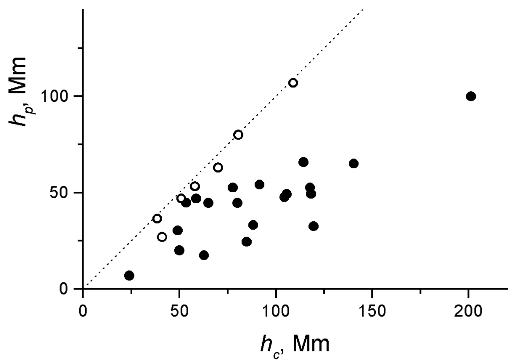

Figure 6. Critical height of stable filament equilibrium h_c versus observed prominence height above the limb h_p. The dotted line corresponding to equality of these quantities is the stability boundary. The solid circles correspond to the filaments which safely passed the west limb. The open circles correspond to the filaments which disappeared from the disk.

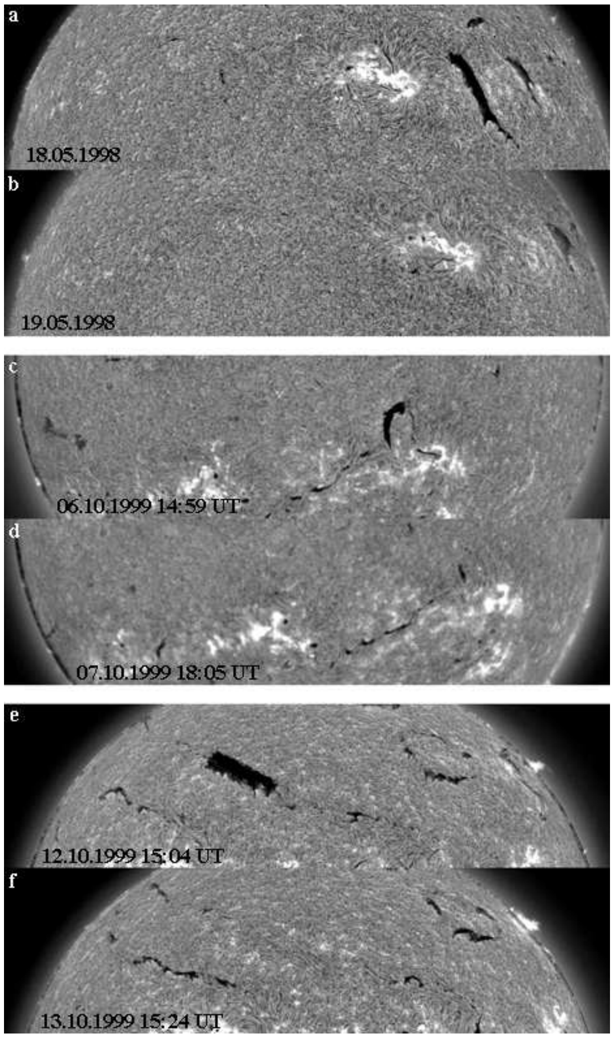

Figure 7. Hα filtergrams demonstrating the filaments disappearance from the disk (Courtesy of Big Bear Solar Observatory).

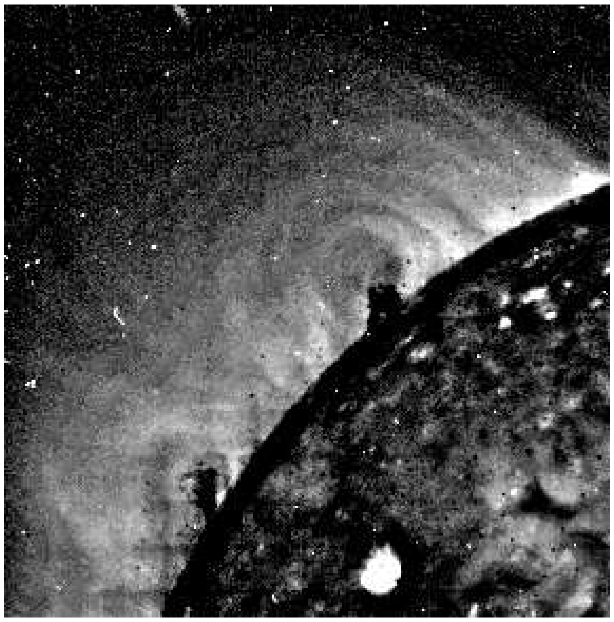

Figure 8. Fragment of the SOHO/EIT image in Fe XV, 284 line on 19 November 1997 showing the ring-like cavity around a prominence and near-circular flux tubes on the border of the cavity. The image was filtered using unsharp mask to reveal the structure. (Courtesy of SOHO/EIT consortium. SOHO is a project of international cooperation between ESA and NASA.)

Table 1. Observed and Calculated Prominence Characteristics

Date of filament crossing of the central meridian	Prominence height, Mm	Limiting height, Mm	Calculated magnetic field strength near the filament, G
16 May 1998	47 ±5	59	8.5
25 May 1998	80	81	1
13 November 1998	100	201	1
1 December 1998	18	63	82
4 December 1998	25	85	15
5 December 1998	7	24	86
26 February 1999	33	120	4.5
24 March 1999	48	105	3.5
8 April 1999	66	115	2
5 May 1999	65	141	3
19 May 1999	34	88	2.5
26 May 1999	54	58	3
7 June 1999	45	54	5
1 July 1999	45	65	6.5
4 July 1999	20	50	5
16 July 1999 (Northern Hemisphere)	53	78	1.5
16 July 1999 (Southern Hemisphere)	50	106	4.5
4 August 1999	27	41	19.5
7 August 1999	50	119	4.5
13 August 1999	45	80	11
15 August 1999	53	118	2
20 August 1999	54	92	8.5
5 October 1999	107	109	1.5
12 October 1999	63	70	1.5
11 January 2000	31	50	6.5
15 March 2000	47	51	23.5
20 April 2000	37	39	2.5